Reactions of Lanthanides and Actinides in Molten Alkali Metal/Polychalcogenide Fluxes at Intermediate Temperatures (250−600 °C)

Anthony C. Sutorik and Mercouri G. Kanatzidis*

Department of Chemistry and Center for Fundamental Materials Research, Michigan State University, East Lansing, Michigan 48824

Received August 26, 1996[⊗]

From the reaction of the elemental lanthanides and actinides in molten alkali metal/polychalcogenide salts, several new ternary compounds have been discovered. Specifically, these phases are K_4USe_8 (I) and $ALnQ_4$ (II), where A = K, Ln = Ce or Tb, and Q = Se or A = Rb, Ln = Ce, Q = Te; and $NaLnS_3$ (III), where Ln = La, Ce. The K_4USe_8 crystallizes in the orthorhombic space group *Fdd*2 (No. 43) with a = 17.331(4) Å, b = 20.584(3) Å, c = 8.811(3) Å, Z = 8. The $KCeSe_4$ crystallizes in the tetragonal space group *P*4/*nbm* (No. 125) with a = 6.376(2) Å, c = 8.327(1) Å, Z = 2. The $KTbSe_4$ crystallizes in the tetragonal space group *P*4/*nbm* (No. 125) with a = 6.255(2) Å, c = 8.227(1) Å, Z = 2. The $RbCeTe_4$ crystallizes in the tetragonal space group *P*4/*nbm* (No. 125) with a = 6.952(3) Å, c = 9.084(4) Å, Z = 2. The $NaCeS_3$ crystallizes in the orthorhombic space group *Pmmn* (No. 59) with a = 5.683(1) Å, b = 4.238(2) Å, c = 9.802(2) Å, Z = 2. The $NaLaS_3$ crystallizes in the orthorhombic space group *Pmmn* (No. 59) with a = 5.752(4) Å, b = 4.2796(6) Å, c = 9.841(2) Å, Z = 2. Compound I features discrete $[U(Se_2)_4]^{4-}$ anions, while (II) and (III) possess extended structures in which the lanthanide and chalcogenide atoms form infinite two-dimensional layers. In II the lanthanide cations are in square antiprismatic coordination environments, connected into layers by Q−Q bonds. In III, the lanthanides bond to a mixture of mono- and disulfides in a bicapped trigonal prismatic geometry; these polyhedra subsequently connect in two dimensions, forming layers equivalent to those seen in the $ZrSe_3$ structure type. Details of the synthesis, structure, and properties of these compounds are discussed.

Introduction

The chemistry between metal cations and polychalcogenide ligands has been studied extensively over the years using a variety of solution-based techniques.[1] This has led to a considerable amount of empirical knowledge concerning the complexes that have resulted, although the complex solution equilibria that polychalcogenides are prone to, based on their ability to undergo self-redox reactions, have made synthetic predictability difficult. In many systems the reaction of metals in molten polychalcogenide salts has been a valuable addendum to theses studies. Because of the unique reaction characteristics of molten A_2Q_x salts,[2] these media have had value in accessing compounds previously unknown even in systems that had been well studied with conventional solution techniques. The new phases seen in molten salt reactions have also tended to be solid-state structures with extended covalent bonding in one or more dimensions through the lattice, a sharp contrast to the discrete ionic complexes commonly resulting from solution.[2] For many elements, however, studying metal/$(Q_x)^{2-}$ chemistry can be exceedingly difficult. Group 4 and 5 transition metals, lanthanides, and actinides can access very high oxidation states and hence become very hard Lewis acids. As such they are especially oxophilic species that, when given a choice, would rather coordinate to oxygen-containing (hard base) ligands rather than those with chalcogenide (soft base) binding sites. Therefore they enjoy a particularly rich oxide chemistry. [3]

By using molten A_2Q_x fluxes, the opportunity presents itself to study the reaction of highly oxophilic metals with polychalcogenide ligands directly, without the need for any sort of polar solvent medium. These fluxes were described by Scheel[4] to be excellent recrystallizing media for many chalcogenides. He also hinted that at lower temperatures new phases containing the alkali atom may form. Some of the earliest investigations into using A_2Q_x fluxes as intermediate temperature media were performed on group 4 and 5 metals. From these studies, the phases $K_4Ti_3S_{14}$,[5] $Na_2Ti_2Se_8$,[6] and $K_3NbNb_2Se_{11}$[7] were identified.

In this work, U has been the only actinide whose reactivity with A_2Q_x fluxes was studied. Several U/Q binaries exist, but the only one to have discrete polychalcogenides is UQ_3 (Q = S, Se, Te),[8] which is isostructural to $ZrSe_3$.[9] This structure type, to be discussed at length later, contains $(Q_2)^{2-}$ fragments which, through

[⊗] Abstract published in *Advance ACS Abstracts,* November 1, 1996.

(1) (a) Flomer, W. A.; Kolis, J. W. *J. Am. Chem. Soc.* **1988**, *110*, 3682−3683. (b) Eichhorn, B. W.; Haushalter, R. C.; Cotton, F. A.; Wilson, B. *Inorg. Chem.* **1988**, *27*, 4084−4085. (c) Kanatzidis, M. G.; Huang, S.-P. *J. Am. Chem. Soc.* **1989**, *111*, 760−761. (d) Kanatzidis, M. G.; Huang, S.-P.; *Angew. Chem., Int. Ed. Engl.* **1989**, *28*, 1513−1514. (e) Kanatzidis, M. G.; Huang, S.-P. *Coord. Chem. Rev.* **1994**, *130*, 509−621. (f) Kolis, J. W. *Coord. Chem. Rev.* **1990**, *105*, 195−219.

(2) Kanatzidis, M. G.; Sutorik, A. C. *Prog. Inorg. Chem.* **1995**, *43*, 151−265 and references therein.

(3) Wells, A. F. *Structural Inorganic Chemistry*, 4th ed.; 1975.

(4) Scheel, H. J. *J. Cryst. Growth* **1974**, *24/25*, 669 and references therein.

(5) Sunshine, S. A.; Kang, D.; Ibers, J. A. *J. Am. Chem. Soc.* **1987**, *109*, 6202−6204.

(6) Kang, D.; Ibers, J. A. *Inorg. Chem.* **1988**, *27*, 549−551.

(7) Schreiner, S.; Aleandri, L. E.; Kang, D.; Ibers, J. A. *Inorg. Chem.* **1989**, *28*, 392−393.

S0897-4756(96)00448-6 CCC: $14.00

η^2 coordination, form the short sides of a trigonal prism around the U atoms.

A brief look at known ternary compounds containing alkali cations is warranted because working with A_2Q_x fluxes naturally can lead to the incorporation of A^+ into the resulting lattice. For alkali metals (and Tl^+) only one stoichiometry had been known for many years: $ALnQ_2$.[10] This phase exists in two different structure types depending on the relative sizes of the A^+ and Ln^{3+} cations. Generally, for small alkali metal cations (Li^+ and some Na^+ analogues), the phase is simply a NaCl derivative with the two cations disordered throughout the lattice. As A^+ increases in size, the cations order themselves in the NaCl lattice such that every other layer of cations changes composition between A^+ and Ln^{3+}. The recent characterization of $RbDy_3Se_8$ has added another structure type to the A/Ln/Q family.[11] This phase is a relative of the $LnTe_3$ structure type modified by (a) a layer of Rb^+ inserted between the double layer of polychalcogenides and (b) partial occupancies in the polyselenide sheets, implying a variety of fragment lengths being stabilized.

As in binary systems, examples of ternary A/actinide/Q phases are sparse. The unit cell has been reported for KUS_3,[12] but the structure could not be successfully refined. Some of the known phases include $Cu_2U_6Q_{13}$,[13] CrU_8S_{17},[14a] MU_8S_{17},[14b] ScU_3S_6,[14c] $ScUS_3$,[14d] $BaUS_3$,[15a] $RhUS_3$,[15b] PdU_2S_4,[15c] and $CaUS_2$[15d] and feature U centers in high coordination environments. Recently, the new phases $CsUTe_6$ and $CsTiUTe_5$ were reported to form from cesium alkali metal polytelluride melts.[16] The compounds discussed have all resulted from high-temperature (>600 °C) solid-state reactions, except for $RbDy_3Se_8$, which was grown from a RbCl/LiCl flux at 680 °C. The solid-state chemistry between these elements has never been reported under any but high-temperature synthetic conditions. The binary lanthanide chalcogenide phases MTe_3 (M = La, Pr) were shown to form at <600 °C in A_2Q_x fluxes.[17] Molten A_2Q_x fluxes, however, allow for a changing of the conditions by varying x, and as we show here, can lead to ternary new phases.[2] The first stage in the investigation of f-block metal reactivity in A_2Q_x fluxes was to experiment on simple ternary systems. The considerable thermodynamic stability of the known binary and ternary compounds often led to their formation even under the relatively mild synthetic temperatures employed here. Despite this, it was discovered that, with appropriate flux compositions, several new ternary chalcogenides can be accessed at intermediate temperatures. The reactivity of some lanthanides and actinides, in combination with Cu containing A_2Q_x fluxes was shown to result in the quaternary compounds $K_2Cu_2CeS_4$, $KCuCe_2S_6$, $KCuLa_2S_6$, $CsCuCe_2S_6$, $KCuCe_2Se_6$, $CsCuCeS_3$, and $KCuUSe_3$.[18] In this paper the syntheses, structures, and properties of the new ternary phases K_4USe_8 (I), $ALnQ_4$ (II) (where A = K, Ln = Ce or Tb, and Q = Se or A = Rb, Ln = Ce, Q = Te), and $NaLnS_3$ (III) (where Ln = La, Ce) will be discussed. Preliminary reports on this work have been published previously.[19]

Experimental Section

Synthesis. *Reagents.* The following reagents were used as obtained: cerium, 40 mesh, Johnson M. Matthey Co., Ward Hill, MA; uranium metal, 60 mesh, Cerac, Milwaukee, WI; lanthanum, 40 mesh, Cerac, Milwaukee, WI; selenium powder, 100 mesh, Aldrich, Milwaukee, WI; tellurium powder, 200 mesh, Aldrich, Milwaukee, WI; sulfur powder, sublimed, JT Baker Co., Philllipsburg, NJ; rubidium metal, analytical reagent, Johnson Matthey, Ward Hill, MA; potassium metal, analytical reagent, Mallinckrodt Inc., Paris, KY; sodium metal, analytical reagent, Mallinckrodt Inc., Paris, KY; dimethylformamide, analytical reagent grade, EM Science, Inc., Gibbstown, NJ. K_2S, K_2Se, and K_2Te were prepared as described previously.[20]

K_4USe_8. This compound was synthesized from a mixture of 0.126 g (0.80 mmol) of K_2Se, 0.095 g (0.40 mmol) of U, and 0.257 g (3.25 mmol) of Se. These reagents are thoroughly mixed, sealed in an evacuated Pyrex ampule, and heated at 300 °C for 12 days (cooling 2 °C/h). Afterward, the tube is opened with a glass cutter, and the entire solid mass is placed in a 250 mL Erlenmeyer flask, which has a sidearm attachment to allow for the purging of the flask contents with N_2. Excess polyselenide flux is removed by dissolving it in successive portions of degassed dimethylformamide (DMF). Approximately 50−100 mL of solvent is added to the flask resulting in a green/brown solution as the excess K_2Se_x is dissolved. Nitrogen flow through the flask is maintained during the isolation to prevent oxidation of the solubilized polychalcogenide by ambient O_2 which would cause elemental Se to precipitate. When a portion of solvent becomes saturated (as evidenced by a very dark color to the solution), it is carefully decanted from the remaining solid, and a fresh portion is added. Since K_4USe_8 has proven to be slightly

(8) (a) Ben Salem, A.; Meerschaut, A.; Rouxel, J. *C. R. Acad. Sci., Paris, Ser. II* **1984**, *299*, 617−619. (b) Noel, H.; Levet, J. C. *J. Solid State Chem.* **1989**, *79*, 28−33.

(9) Kronert, V. W.; Plieth, K. *Z. Anorg. Allg. Chem.* **1965**, *336*, 207−218.

(10) Compounds of the type $ALnQ_2$ (A = Na; Ln = La, Ce, Pr, Nd; Q = S) were first synthesized by Ballestracci and Bertaut with the range of compounds expanded to include A = Li, K, Rb, Cs; Q = Se; and several other Ln metals by themselves and others. (a) Ballestracci, R.; Bertaut, E. F. *Bull. Soc. Fr. Mineral. Crystallogr.* **1964**, *87*, 512−516. (b) Ballestracci, R.; Bertaut, E. F. *Bull. Soc. Fr. Mineral. Crystallogr.* **1965**, *88*, 136−141. (c) Ballestracci, R. *Bull. Soc. Fr. Mineral. Crystallogr.* **1965**, *88*, 207−210. (d) Tromme, M. *C. R. Acad. Sci. Ser. C* **1971**, *273*, 849−853. (e) Bronger, W.; Elter, R.; Schmidt, E. *Rev. Chim. Miner.* **1974**, *10*, 147−152. (f) Kabre, S.; Julien-Pouzol, M.; Guittard, M. *Bull. Soc. Chim. Fr.* **1974**, *10*, 1881−1884. (g) Plug, C. M.; Verschoor, G. C. *Acta Crystallogr.* **1976**, *B32*, 1856−1858. (h) Ohtani, T.; Honjo, H.; Wada, H. *Mater. Res. Bull.* **1987**, *22*, 829−840. (i) Bronger, W. *Crystallography and Crystal Chemistry of Materials with Layered Structures*; Levy, F., Ed.; D. Reidel Publishing Company: Dordrecht, Holland, 1976; p 93. (j) Brunel, M.; DeBergevin, F.; Gondrand, M. *J. Phys. Chem. Solids* **1972**, *33*, 1927−1941.

(11) Foran, B.; Lee, S.; Aronson, M. *Chem. Mater.* **1993**, *5*, 974−978.

(12) Padiou, J.; Guillevic, J. *C. R. Hebd. Seances Acad. Sci. Ser. C* **1969**, *268*, 822−824.

(13) (a) Noel, H.; Potel, M. *J. Less Common Met.* **1985**, *113*, 11−15. (b) Noel, H. *J. Less Common Met.* **1980**, *72*, 45−49.

(14) (a) Noel, H.; Padiou, J. *Acta Crystallogr. B* **1976**, *32*, 1593−1595. (b) Noel, H.; Troc, R. *J. Solid State Chem.* **1979**, *27*, 123−135. (c) Rodier, N.; Tien, V. *Acta Crystallogr. B* **1976**, *32*, 2705−2707. (d) Julien, R.; Rodier, N.; Tien, V. *Acta Crystallogr. B* **1978**, *34*, 2612−2614.

(15) (a) Brochu, R.; Padiou, J.; Grandjean, D. *C. R. Hebd. Seances Acad. Sci.* **1970**, *271*, 642−643. (b) Daoudi, A.; Noel, H. *Inorg. Chim. Acta* **1987**, *140*, 93−95. (c) Daoudi, A.; Noel, H. *J. Less Common Met.* **1986**, *115*, 253−259. (d) Komac, M.; Golic, L.; Kolar, D.; Brcic, B. S. *J. Less Common Met.* **1971**, *24*, 121−128.

(16) Cody, J. A.; Ibers, J. A. *Inorg. Chem.* **1995**, *34*, 3165.

(17) Chen, J. H.; Dorhout, P. K. *J. Solid State Chem.* **1995**, *117*, 318−322.

(18) (a) Sutorik, A. C.; Albritton-Thomas, J.; Kannewurf, C. R.; Kanatzidis, M. G. *J. Am. Chem. Soc.* **1994**, *116*, 7706−7713. (b) Sutorik, A. C.; Albritton-Thomas, J.; Hogan, T.; Kannewurf, C. R.; Kanatzidis, M. G. *Chem. Mater.* **1996**, *8*, 751−761.

(19) (a) Sutorik, A. C.; Kanatzidis, M. G. *J. Am. Chem. Soc.* **1991**, *113*, 7754−7755. (b) Sutorik, A. C.; Kanatzidis, M. G. *Angew. Chem., Int. Ed. Engl.* **1992**, *31*, 1594−1596.

(20) (a) McCarthy, T. J.; Ngeyi, S.-P.; Liao, J.-H.; DeGroot, D.; Hogan, T.; Kannewurf, C. R.; Kanatzidis, M. G. *Chem. Mater.* **1993**, *5*, 331−340. (b) Zhang, X.; Park, Y; Hogan, T.; Schindler, J.; Kannewurf, C. R.; Seong, S.; Albright, T.; Kanatzidis, M. G. *J. Am. Chem. Soc.* **1995**, *117*, 10300−10310.

soluble in DMF, washing is continued only until the green/brown color of an Se_x^{2-} solution is replaced by a slowly evolving brown/yellow color, indicating K_4USe_8 as the primary component in solution. The sample is decanted one final time and then dried under vacuum. The remaining material is a black microcrystalline product. Homogeneity was confirmed by comparing the powder X-ray diffraction pattern of the product against one calculated using X-ray single-crystal data (see Supporting Information). Solubility is slow enough that yields as high as 53% have been achieved (based on uranium).

$KCeSe_4$. This compound was synthesized from a reaction of 0.078 g of K_2Se (0.5 mmol), 0.035 g of Ce (0.25 mmol), and 0.158 g of Se (2 mmol). These starting materials are thoroughly mixed in a nitrogen atmosphere glovebox and loaded into a Pyrex tube, which is subsequently evacuated to approximately 2×10^{-3} mbar and flame sealed. The mixture is heated at 300 °C for 6 days and cooled at 2 °C/h to 100 °C followed by cooling to 50 °C in 1 h. The product is isolated in the manner described for the isolation of K_4USe_8 above. The remaining material is deep blue-to-black square chunks of $KCeSe_4$. The product is insoluble in DMF and is inert in both air and water for extended periods, although some manner of surface degradation appears to be evident in the magnetic susceptibility studies. Homogeneity was confirmed by comparing the calculated and observed powder X-ray diffraction patterns. A yield of 60%, based on Ce, is typical.

$KTbSe_4$. This compound was synthesized from a reaction of 0.039 g (0.25 mmol) of K_2Se, 0.040 g (0.25 mmol) of Tb, and 0.160 g (2 mmol) of Se. These starting materials are thoroughly mixed in a nitrogen atmosphere glovebox and loaded into a Pyrex tube, which is subsequently evacuated to approximately 2×10^{-3} mbar and flame sealed. The mixture is heated at 350 °C for 5 days and cooled at 2 °C/h to 100 °C followed by cooling to 50 °C in 1 h. The product is isolated in the manner described for the isolations above. The remaining material is deep purple-to-black square chunks of $KTbSe_4$. The product is insoluble in DMF and is inert in both air and water for extended periods. Homogeneity is confirmed as described above. A yield of 84%, based on Tb, is typical.

$RbCeTe_4$. This compound has been observed and structurally characterized, but attempts to repeat the reaction have, to date, not been successful. Rather, an unknown microcrystalline ternary compound continually appears, and so $RbCeTe_4$ must be a very kinetically sensitive phase.

The original batch of $RbCeTe_4$ resulted from a mixture of 0.149 g (0.50 mmol) of Rb_2Te, 0.035 g (0.25 mmol) of Ce, and 0.255 g (2 mmol) of Te. These starting materials are thoroughly mixed in a nitrogen atmosphere glovebox and loaded into a Pyrex tube, which is subsequently evacuated to approximately 2×10^{-3} mbar and flame sealed. The mixture is heated at 420 °C for 4 days and cooled to 230 °C in 95 h followed by cooling to 130 °C in 20 h and then to 50 °C in 1 h. Black square chunks of $RbCeTe_4$ and some elemental Te were obtained. The product was insoluble in DMF and is inert in both air and water for extended periods. The calculated and observed powder X-ray diffraction patterns for $RbCeTe_4$ are given in the Supporting Information.

$NaCeS_3$. This compound was first observed from an attempted heterometallic reaction of Cu and Ce in a molten Na_2S_x flux. 0.234 g (3.0 mmol) of Na_2S, 0.016 g (0.25 mmol) of Cu, 0.036 g (0.26 mmol) of Ce, and 0.256 g (8.0 mmol) of S were thoroughly mixed in a nitrogen atmosphere glovebox and loaded into Pyrex tubes, which were subsequently evacuated to approximately 2×10^{-3} mbar and flame sealed. The reaction was heated at 400 °C for 5 days and cooled at 4 °C/h to 120 °C followed by cooling to 50 °C in 1 h. The product is isolated by dissolving away the excess polysulfide flux with several portions of degassed dimethylformamide (DMF) as described earlier. Concentrated solutions of $(S_x)^{2-}$ in DMF have a blue color, and so washings are continued until the solvent remains clear, indicating total polysulfide removal. The resulting product was an inhomogeneous mixture of red needles and black and orange powder. Semiquantitative EDS analysis revealed a Na/Ce/S composition of 2/3/8 for the red needles and a Cu/Ce/S ratio of 1/1/1 for the black powder. Single-crystal X-ray diffraction studies were subsequently performed on the red needles from this synthesis, leading to the structure of $NaCeS_3$.

Rational synthesis of pure $NaCeS_3$ was achieved from two different ratios of starting materials. Either a mixture of 0.078 g (1.0 mmol) of Na_2S, 0.070 g (0.5 mmol) of Ce, and 0.096 g (3.0 mmol) of S or 0.040 g (0.5 mmol) of Na_2S, 0.070 g (0.5 mmol) of Ce, and 0.064 g (2.0 mmol) of S can be used. Both have in common that the resulting fluxes (Na_2S_5 and 2 Na_2S_4) are fairly Lewis basic and are present in only a moderate excess to the Ce metal. After being mixed and sealed into Pyrex tubes as described earlier, the reactants are heated to 370 °C over 12 h, held at that temperature for 2 days, and then cooled to 160 °C over 50 h followed by quenching to room temperature. The excess flux is removed using degassed DMF as described above. The resulting brick red powder was confirmed as $NaCeS_3$ by X-ray powder diffraction. The material is insoluble in DMF and appears to be stable in dry air. However, $NaCeS_3$ is extremely moisture sensitive; any contact with water turns the entire sample black, which is seen by powder X-ray diffraction to contain CeO_2. Even ambient air has sufficient humidity to form a black surface coating over a short period of time, although the coating seems to be protective of the internal compound as its relative amount does not increase with longer exposure to the atmosphere.

$NaLaS_3$. Either of the following combinations of starting materials may be used to form $NaLaS_3$: 0.060 g (0.77 mmol) of Na_2S, 0.105 g (0.75 mmol) of La, and 0.096 g (3.0 mmol) of S; or 0.117 g (1.5 mmol) of Na_2S, 0.105 g (0.75 mmol) of La, and 0.144 g (4.5 mmol) of S. The former resulted in crystals suitable for single-crystal X-ray diffraction studies, while the latter is typically microcrystalline. The starting materials are mixed and sealed into Pyrex tubes as described previously. The samples are placed in a computer controlled furnace and heated to 370 °C over 12 h. They remain at this temperature for 2 days after which the furnace is cooled to 160 °C over 50 h and then allowed to cool naturally to 50 °C. The excess flux is dissolved by washing the sample with degassed DMF as described previously. The isolated product is pale yellow when microcrystalline but orange as the size of the crystals increases. Purity of the sample was confirmed by comparing its X-ray powder diffraction pattern to one calculated from the single-crystal diffraction data. $NaLaS_3$ is highly stable in air and common organic solvents and remains intact in H_2O over short periods of time (<8 h). After sufficient contact with water, the phase converts to an amorphous oxide with the scent of H_2S present.

Physical Measurements. *Powder X-ray Diffraction.* Analyses were performed using a calibrated Rigaku Rotaflex rotating anode powder diffractometer controlled by an IBM computer and operating at 45 kV/100 mA, employing Ni-filtered Cu radiation. Samples are ground to a fine powder and mounted by spreading the sample onto a piece of double-sided scotch tape affixed to a glass slide. For air-sensitive compounds, samples were prepared in an N_2-filled glovebox and coated with mineral oil before analysis. Powder patterns were calculated by using the CERIUS molecular modeling program by Molecular Simulations, St. John's Innovation Centre, Cambridge, England.

Infrared Spectroscopy. Infrared spectra, in the far-IR region (600−50 cm^{-1}), were recorded on a computer-controlled Nicolet-740 Fourier transform infrared spectrophotometer in 4 cm^{-1} resolution. Analyses were performed on finely ground solid samples using CsI as the pressed pellet matrix. For air-sensitive compounds, samples were prepared in an N_2-filled glovebox and pressed into a pellet immediately upon removal.

Solution UV/Vis Spectroscopy. Spectra were recorded using a Hitachi U-2000 spectrophotometer. Samples were dissolved and loaded into UV/vis cells inside an N_2-filled glovebox.

Solid-State UV/Vis/Near-IR Spectroscopy. Optical diffuse reflectance measurements were performed at room temperature using a Shimadzu UV-3101PC double-beam, double-monochromator spectrophotometer. The instrument is equipped with an integrating sphere and controlled by personal computer. The reflectance versus wavelength data generated can be used to estimate a material's bandgap by converting

Table 1. Crystallographic Data for K_4USe_8, $KCeSe_4$, $KTbSe_4$, $RbCeTe_4$, $NaCeS_3$, and $NaLaS_3$

	K_4USe_8	$KCeSe_4$	$KTbSe_4$	$RbCeTe_4$	$NaCeS_3$	$NaLaS_3$
FW, g/mol	1026.10	495.06	513.86	735.99	259.29	258.08
a, Å	17.331(4)	6.376(2)	6.255(2)	6.952(3)	5.683(1)	5.752(4)
b, Å	20.584(3)				4.238(2)	4.2796(6)
c, Å	8.811(3)	8.327(1)	8.227(3)	9.084(4)	9.802(2)	9.841(2)
β, deg	90.0	90.0	90.0		90.0	90.0
V, Å^3	3143(1)	338.6(2)	321.9(2)	439.0(6)	236.0(2)	242.2(3)
space group	*Fdd*2 (No. 43)	*P*4/*nbm* (No. 125)	*P*4/*nbm* (No. 125)	*P*4/*nbm* (No. 125)	*Pmmn* (No. 59)	*Pmmn* (No. 59)
Z	8	2	2	2	2	2
d_{calc}, g/cm^3	4.336	4.855	5.301	5.567	3.648	2.538
μ, cm^{-1}	291.7	286	340.23	236.07	109.69	99.95
crystal dimensions, mm^3	1.0 × 1.0 × 1.0	0.02 × 0.08 × 0.08	0.04 × 0.42 × 0.46	0.01 × 0.07 × 0.08	0.01 × 0.04 × 0.44	0.02 × 0.26 × 0.40
radiation	Mo Kα	Mo Kα	Mo Kα	Mo Kα	Mo Kα	Mo Kα
2θ max, deg	50	60	60	55	60	60
data collection temp, °C	23	23	23	20	−75	23
no. of data collected	797	916	343	623	432	450
no. of unique data	797	251	323	290	432	450
no. of $F_o^2 > 3\sigma(F_o^2)$	647	157	235	197	380	411
no. of variables	60	12	12	9	19	19
R/R_w, %[a]	3.6/4.7	3.0/3.4	4.0/5.1	3.1/2.4	1.9/2.6	2.6/3.4
final dif map max peak, e$^-$/Å^3	3.35	1.18	2.0	1.69	0.61	1.47

[a] $R = \sum(|F_o| - |F_c|)/\sum|F_o|$. $R_w = \{\sum w(|F_o| - |F_c|)^2/\sum w|F_o|^2\}^{1/2}$. The reflections were weighted according to $w = 1/[\sigma(F_o^2)^2 + (0.03F_o^2)^2]^{1/2}$ (where w = weight of a given F_o).

reflectance to absorption data according to a protocol reported earlier.[20a]

Magnetic Susceptibility. The magnetic response of the compounds was measured over the range 2−300 K using a MPMS Quantum Design SQUID magnetometer. Samples were ground to a fine powder to minimize possible anisotropic effects and loaded into PVC containers. Air sensitive samples were prepared as described above. Corrections for the diamagnetism of the PVC sample containers were made by measuring the magnetic response of the empty container under the same conditions of temperature and field which were measured for the filled container. Core atom diamagnetism was much smaller than the magnitude of the paramagnetism measured and so was ignored. Magnetic susceptibility as a function of field strength (at a constant temperature of 300 K) was first investigated to determine if the samples experienced saturation of their magnetic signal. For all compounds, magnetization increased linearly with increasing field over the range investigated (100−55 000 G). The subsequent temperature-dependent studies were performed at low-to-moderate field strengths (300−5000 G).

Single-Crystal X-ray Diffraction. Intensity data were collected using a Rigaku AFC6S four-circle automated diffractometer equipped with a graphite crystal monochromator. An $\omega-2\theta$ scan mode was used. The stability of the crystals was monitored with three standard reflections whose intensities were checked every 150 reflections, and, unless noted, no crystal decay was detected. An empirical absorption correction based on ψ scans was applied to all data during initial stages of refinement. An empirical DIFABS correction[21a] was applied after full isotropic refinement, after which full anisotropic refinement was performed. The structures were solved by direct methods using either MITHRIL[21b] (in the case of K_4USe_8) or SHELXS-86 software[21c] (for all other compounds), and full-matrix least-squares refinement was performed using the TEXSAN software package.[21d] Crystallographic data for the compounds in this report are given in Table 1, and fractional atomic coordinates in Tables 2−4.

Results and Discussion

K_4USe_8. *Structure.* A single $[USe_8]^{4-}$ anion is shown in Figure 1, with selected bond distances and angles in Table 5. The uranium center sits on a crystallographic 2-fold axis, but the entire anion has a triangulated dodecahedral geometry and can hence be assigned a pseudo-D_{2d} symmetry. A dodecahedral structure is characterized by the location of coordinating atoms at the corners of two trapezoids which lie orthogonal to each other; in $[USe_8]^{4-}$ the Se−Se bonds form the nonparallel sides of their respective trapezoids. The $[USe_8]^{4-}$ is distorted from an ideal dodecahedron in two respects. First, the bases of the Se trapezoids intersect

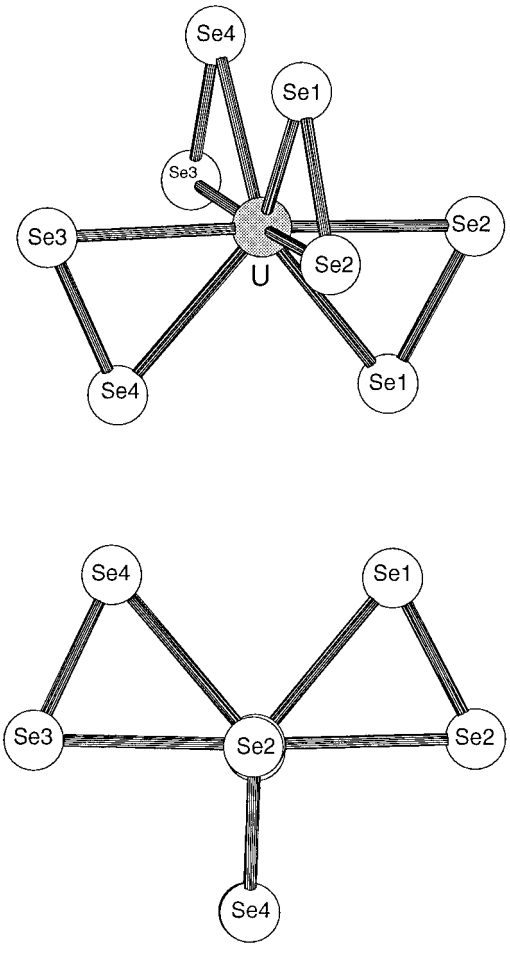

Figure 1. Two views of the structure of the $[U(Se_2)_4]^{4-}$ anion.

(21) (a) Walker, N.; Stuart, D. *Acta Crystallogr.* **1983**, *A39* , 158−166. (b) Gilmore, G. J. *J. Appl. Crystallogr.* **1984**, *17*, 42−46. (c) Sheldrick, G. M. In *Crystallographic Computing 3*; Sheldrick, G. M., Kruger, C., Doddard, R., Eds.; Oxford University Press: Oxford, England, 1985; pp 175−189. (d) TEXSAN: Single-Crystal Structure Analysis Software, Version 5.0, 1981. Molecular Structure Corp.: The Woodlands, TX 77381.

Table 2. Fractional Atomic Coordinates and B_{eq}[a] Values for K_4USe_8 with Estimated Standard Deviations in Parentheses

atom	*x*	*y*	*z*	*B*(eq)
U	1	0	0.0217	0.72(5)
Se(1)	1.0379(2)	0.1198(1)	−0.1197(4)	1.9(1)
Se(2)	1.1100(2)	0.0303(1)	−0.2165(4)	1.6(1)
Se(3)	1.1119(2)	0.0244(1)	0.2633(4)	1.7(1)
Se(4)	1.1051(2)	−0.0869(1)	0.1827(4)	1.5(1)
K(1)	0.9981(4)	0.2741(3)	−0.2415(8)	2.3(3)
K(2)	1.2211(4)	0.1662(3)	−0.2042(8)	2.1(3)

[a] *B* values for anisotropically refined atoms are given in the form of the isotropic equivalent displacement parameters defined as $B_{eq} = {}^4/_3[a^2B(1,1) + b^2B(2,2) + c^2B(3,3) + ab(\cos\gamma)B(1,2) + ac(\cos\beta)B(1,3) + bc(\cos\alpha)B(2,3)]$.

Table 3. Fractional Atomic Coordinates and B_{eq}[a] Values for $KCeSe_4$, $KTbSe_4$, and $RbCeTe_4$ with Estimated Standard Deviations in Parentheses

atom	*x*	*y*	*z*	*B*(eq)[a]
Ce	$^1/_4$	$^1/_4$	0	0.78(5)
Se	−0.1178(2)	0.1178	0.2162(2)	1.04(5)
K	$-^3/_4$	$^1/_4$	$^1/_2$	2.0(2)
Tb	$^1/_4$	$^1/_4$	$^1/_2$	0.60(3)
Se	0.1148(2)	0.6148(1)	0.7091(1)	0.76(3)
K	$^1/_4$	$^1/_4$	0	1.5(1)
Ce	$^1/_4$	$^1/_4$	$^1/_2$	0.59(4)
Te	0.6123(9)	0.1055(9)	0.2911(1)	0.78(4)
Rb	$^1/_4$	$^1/_4$	0	1.81(8)

[a] *B* values for anisotropically refined atoms are given in the form of the isotropic equivalent displacement parameters defined as $B_{eq} = {}^4/_3[a^2B(1,1) + b^2B(2,2) + c^2B(3,3) + ab(\cos\gamma)B(1,2) + ac(\cos\beta)B(1,3) + bc(\cos\alpha)B(2,3)]$.

Table 4. Fractional Atomic Coordinates and B_{eq}[a] Values for $NaLaS_3$ with Estimated Standard Deviations in Parentheses

atom	*x*	*y*	*z*	*B*(eq)[a]
La	$^1/_4$	$^1/_4$	0.12835(3)	0.83(2)
S(1)	$-^1/_4$	$^1/_4$	0.0658(2)	0.94(5)
S(2)	0.4332(2)	$-^1/_4$	0.3198(1)	1.56(5)
Na	$^3/_4$	$^1/_4$	0.3963(4)	2.1(1)
Ce	$^3/_4$	$^1/_4$	0.37187(4)	0.49(2)
S(1)	$^1/_4$	$^1/_4$	0.4355(2)	0.63(6)
S(2)	0.5648(2)	$-^1/_4$	0.1821(1)	1.02(4)
Na	$^1/_4$	$-^3/_4$	0.1015(3)	1.3(1)

[a] *B* values for anisotropically refined atoms are given in the form of the isotropic equivalent displacement parameters defined as $B_{eq} = {}^4/_3[a^2B(1,1) + b^2B(2,2) + c^2B(3,3) + ab(\cos\gamma)B(1,2) + ac(\cos\beta)B(1,3) + bc(\cos\alpha)B(2,3)]$.

Table 5. Selected Bond Distances (Å) and Angles (deg) for K_4USe_8 with Standard Deviations in Parentheses

U−Se(1)	2.840(3)	Se(3)−Se(4)	2.401(4)
U−Se(2)	2.903(3)	Se(1)−K(1)	3.421(7)
U−Se(3)	2.923(3)	Se(1)−K(2)	3.398(7)
U−Se(4)	2.920(3)	Se(2)−K(2)	3.398(7)
Se(1)−Se(2)	2.385(4)	K(1)− K(2)	4.468(9)
Se(1)−U−Se(1)′	127.9(1)	Se(2)−U−Se(4)	94.19(8)
Se(1)−U−Se(2)	49.05(8)	Se(2)−U−Se(4)′	129.00(8)
Se(1)−U−Se(2)′	91.19(9)	Se(3)−U−Se(3)′	86.5(1)
Se(1)−U−Se(3)	90.96(9)	Se(3)−U−Se(4)	48.54(8)
Se(1)−U−Se(3)′	128.48(9)	Se(3)−U−Se(4)′	87.41(9)
Se(1)−U−Se(4)	126.93(9)	Se(4)−U−Se(4)′	121.9(1)
Se(1)−U−Se(4)′	79.95(9)	U−Se(1)−Se(2)	66.8(1)
Se(2)−U−Se(2)′	87.4(1)	U−Se(2)−Se(1)	64.1(1)
Se(2)−U−Se(3)	93.10(8)	U−Se(3)−Se(4)	65.7(1)
Se(2)−U−Se(3)′	177.51(9)	U−Se(4)−Se(3)	65.8(1)

at the U center, leaving the four basal selenium atoms in a nearly square-planar arrangement; in an ideal dodecahedron the trapezoids slice further into each other. Second, the presence of the Se−Se bonds, although slightly elongated (2.38 and 2.40 Å), necessitates that the corresponding Se−U−Se angle be smaller than in an ideal dodecahedron (Se(1)−U−Se(2) angle 49.05°; corresponding ideal dodecahedron angle 73.69°). Although without precedent in metal−chalcogenide systems, $[USe_8]^{4-}$ is isostructural (but not isoelectronic) with the known peroxo anions $([M(O_2)_4]^{n-})$[22] (M = Cr^{5+}, V^{5+}, Nb^{5+}, Ta^{5+}, Mo^{6+}, W^{6+}).

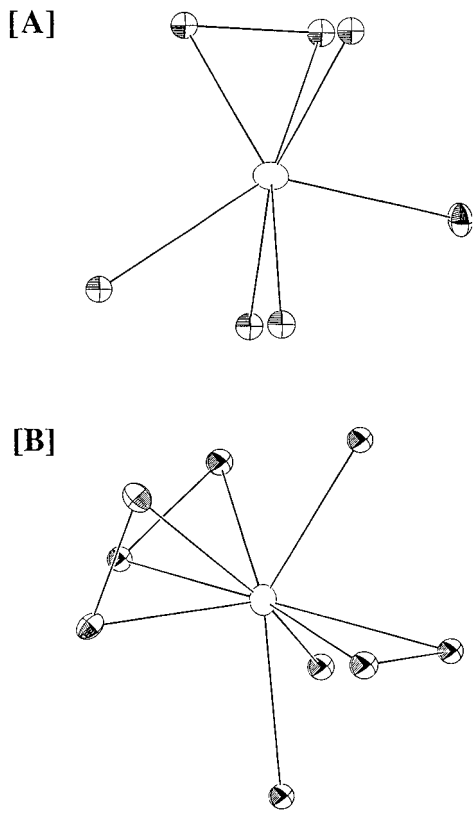

Figure 2. Ortep drawings of the coordination environments of the atoms K(1) (A) and K(2) (B) in the structure of K_4USe_8.

The potassium cations are located in two different sites. The first is coordinated by seven Se atoms in an irregular polyhedron (Figure 2a; range of K(1)−Se distances 3.475(7) Å−3.190(7) Å; ave 3.357 Å) while the second is in a site coordinated by nine Se atoms, again in an irregular polyhedron (Figure 2b; range of K(2)−Se distances 3.694(8) Å−3.253(7) Å; ave 3.470 Å). Examples of molecular uranium/chalcogenide complexes are sparse. A fully characterized homoleptic uranium thiolate has been recently reported.[23] Prior to this, most work has dealt with complexes of uranyl with various sulfur containing ligands,[24] including a complex containing a single η^2-S_2^{2-}.[25]

(22) (a) Stomberg, R. *Acta Chem. Scand.* **1969**, *23*, 2755−2763. (b) Stomberg, R. *Acta Chem. Scand.* **1963**, *17*, 1563−1566. (c) Mathern, G.; Weiss, R. *Acta Crystallogr.* **1971**, *B27*, 1598−1609. (d) Stomberg, R. *J. Less Common Met.* **1988**, *143*, 363−371.

(23) Tatsumi, K.; Matsubara, I.; Inoui, Y.; Nakamura, A.; Cramer, R.; Tagosi, G.; Golen, J.; Gilje, J. *Inorg. Chem.* **1990**, *29*, 4928−4938.

(24) (a) Perry, D. L. *Inorg. Chim. Acta* **1978**, *48*, 117−124. (b) Perry, D. L.; Templeton, D. H.; Zalkin, A. *Inorg. Chem.* **1978**, *17*, 3699−3701. (c) Bowman, K.; Dori, Z. *J. Chem. Soc., Chem. Commun.* **1968**, 636. (d) Graziani, R.; Zarli, B.; Cassol, A.; Bombieri, G.; Forsellini, E.; Tondello, E. *Inorg. Chem.* **1970**, *9*, 2116−2124. (e) Bagnall, K. W.; Holah, D. G. *Nature (London)* **1967**, *215*, 623. (f) Bagnall, K. W.; Brown, D.; Holah, D. G. *J. Chem. Soc. A* **1968**, 1149−1153. (g) Bibler, J. P.; Karraker, D. G. *Inorg. Chem.* **1968**, *7*, 982−985. (h) Bombieri, G.; Croatto, U.; Forsellini, E.; Zarli, B.; Graziani, R. *J. Chem. Soc., Dalton Trans.* **1972**, 560−564. (i) Ryan, R. R.; Smith, B. F.; Ritchey, J. M. *Inorg. Chim. Acta* **1987**, *129*, 139−148.

(25) Perry, D.; Zalkin, A.; Ruben, H.; Templeton, D. H. *Inorg. Chem.* **1982**, *21*, 237−240.

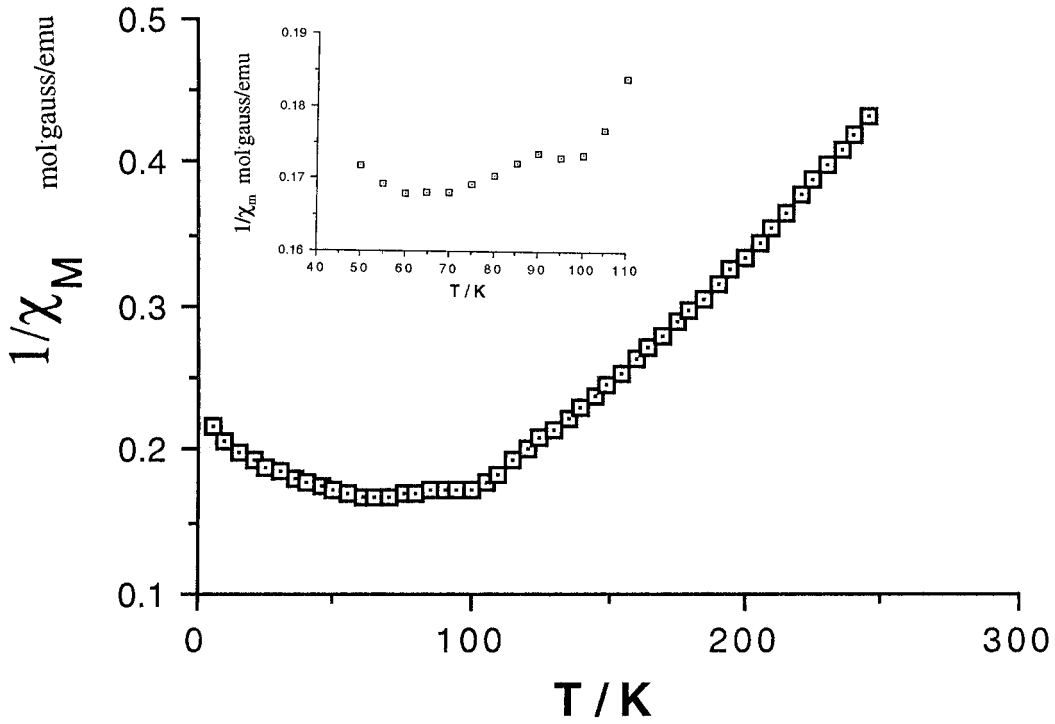

Figure 3. Inverse molar magnetic susceptibility ($1/\chi_M$) plotted against temperature (K) for K_4USe_8 (5000 G).

Magnetic Properties. The magnetic susceptibility of K_4USe_8 was measured as a function of temperature (5−250 K) at a constant field of 5000 G. A plot of the data as $1/\chi_M$ vs T is shown in Figure 3. Strong paramagnetic behavior, conforming to Curie−Weiss law, is observed from approximately 120 K on up. Below this region, a transition is observed at approximately 90 K and is then followed by antiferromagnetic ordering which has a critical temperature of 65 K at the midpoint of a broad and shallow transition. The μ_{eff} at 300 K is 3.82 μ_B, consistent with an f^2 configuration where $L \neq 0$.[26] The exhibited paramagnetic behavior of the compound at high temperatures renders difficult any ^{77}Se NMR study of this compound. Antiferromagnetic transitions of various degrees have been reported for the uranium compounds MU_8Q_{17} (M = Cr, V, Co, Fe, Ni) by Noel and Troc,[14] although their data are complicated by the presence of M^{2+}. Neither K^+ nor Se_2^{2-} would contribute to any magnetic phenomenon, and so barring any impurity, we are observing behavior based solely on U^{4+}.

Spectroscopy. The solid-state far-IR spectrum of K_4USe_8 shows three peaks: 261 cm^{-1}, which can be tentatively assigned to Se−Se stretching in the diselenide groups, 168 and 153 cm^{-1} which are presumably due to U−Se vibrations.

As mentioned before K_4USe_8 is slowly soluble in DMF, and similar behavior has been found with ethylenediamine. The compound was insoluble in neat acetonitrile, even with the addition of $[Bu_4N]^+$; however, it was successfully dissolved in solutions of either $(CH_2CH_2O)_5$ (15C5) or $(CH_2CH_2O)_6$ (18C6) crown ethers, or 2,2,2-cryptand in CH_3CN.

In all solvents the solutions of K_4USe_8 gave brown/yellow colors of various hues which were stable, by UV/vis, out to 3 days. The DMF and CH_3CN/complexant solutions gave similar UV/vis spectra: one broad plateau at 400−430 nm for DMF and at 390−430 nm for CH_3CN/complexant. After decomposition the solutions revert to brown/green in color, and their UV/vis spectra show the features of a polyselenide solution (peaks at 440 and 640 nm for DMF, 417 and 560 nm for CH_3CN). Such a decomposition takes place in all solvents tested upon exposure to air, and simply upon standing, due to the high oxophilicity of U(IV), making distilled and degassed solvents a requirement. In ethylenediamine solutions of K_4USe_8, UV/vis shows peaks at 346, 404, 492, and 807 nm, while a polyselenide/ethylenediamine solution shows peaks at 408, 560, and 805 nm. Although clearly not a simple Se_x^{2-} solution, the presence of several peaks in the ethylenediamine solution indicates a significantly stronger solvent interaction with the anion than in either DMF or CH_3CN.

$ALnQ_4$ (A = K; Ln = Ce, Tb; Q = Se or A = Rb; Ln = Ce; Q = Te). *Structure.* In the $ALnQ_4$ structure, Ln and Q form two-dimensional anionic layers with A^+ in the interlayer gallery. The anionic layers themselves are further partitioned into two layers of $(Q_2)^{2-}$ units sandwiching a layer of Ln^{3+} cations. The Ln^{3+} cations are in a square antiprismatic environment, coordinated to the ends of eight dichalcogenides, four above the Ln plane and four below. A view of this arrangement is shown in Figure 4. Selected bond distances and angles are given in Table 6. It can be seen that the $(Se_2)^{2-}$ units point in a uniform direction within their layer and invert that direction in the layer below. Each $(Se_2)^{2-}$, in turn, bridges four Ln^{3+} cations in a symmetrical μ_2:μ_2 fashion. The expanded anionic layer is shown in Figure 5. Except for the expected changes in bond distances, the $RbCeTe_4$ analogue is almost perfectly isostructural, with the respective bond angles being comparable to those in the selenides. Table 6 lists the bond distances and angles of the telluride.

(26) Figgis, B. N. In *Introduction to Ligand Fields*; Interscience Publishers: New York, 1966.

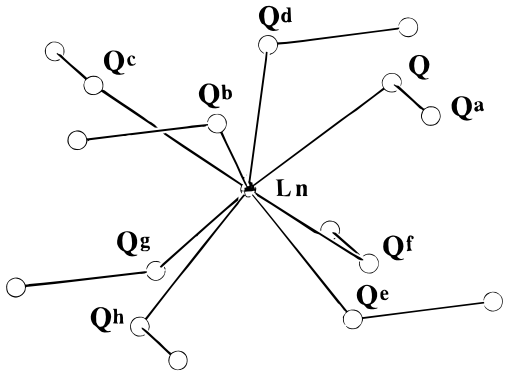

Figure 4. Immediate coordination environment of the Ln^{3+} cations in the ALnQ4 structure type (A = alkali, Ln = lanthanide, Q = Se, Te).

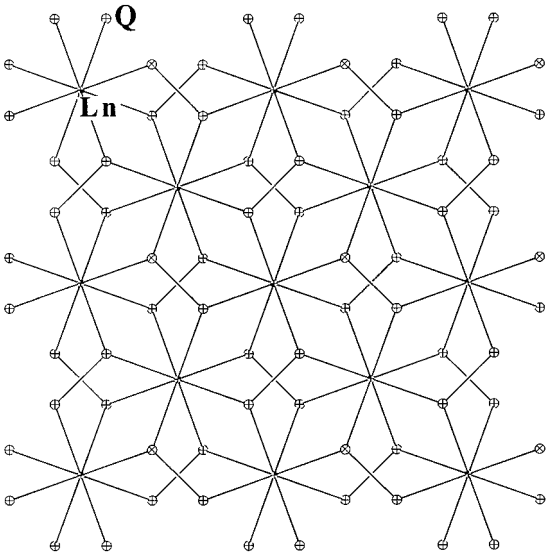

Figure 5. View perpendicular to the anionic layers of $ALnQ_4$.

Table 6. Selected Bond Distances (Å) and Angles (deg) for $KCeSe_4$, $KTbSe_4$, and $RbCeTe_4$ with Standard Deviations in Parentheses

AMQ_4	$KCeSe_4$	$KTbSe_4$	$RbCeTe_4$
M−Q	3.075(1)	2.980(1)	3.285(1)
M−A	4.1646(7)	4.114(1)	4.542(2)
Se−Se[a]	2.385(3)	2.393(2)	3.285(1)
Se−A	3.434(2)	3.414(2)	3.765(1)
A−A[a]	4.509(1)	4.423(2)	4.916(2)
Q−M−Q[b]	69.92(3)	70.55(4)	70.50(2)
Q−M−Q[c]	108.27(7)	109.51(6)	109.40(5)
Q−M−Q[d]	69.92(3)	70.55(3)	70.50(2)
Q−M−Q[e]	80.61(7)	80.06(6)	81.16(4)
Q−M−Q[f]	85.70(7)	84.15(6)	83.1(4)
Q−M−Q[g]	148.17(5)	147.00(3)	145.23(2)
Q−M−Q[h]	139.60(6)	140.17(4)	141.97(2)
M−Q−Q[a]	110.20(3)	109.92(5)	109.01(1)
M−Q−Q[a]	94.30(5)	95.85(5)	96.89(4)

A further feature of this structure is that in the direction parallel to (110), channels are formed, bounded on the opposite sides by Ln^{3+} and on the top and bottom by $(Q_2)^{2-}$ (Figure 6). Their dimensions are 4.16 Å (Ce to Ce) by 3.61 Å (Se to Se) in $KCeSe_4$, with the analogous dimensions in $KTbSe_4$ being 4.11 and 3.64 Å and in $RbCeTe_4$, 4.92 and 4.25 Å. Hence they present too small of a volume for intercalation of most species, although Li intercalation may be a possibility via reduction of $(Q_2)^{2-}$ to $2Q^{2-}$.

The A^+ cations of the structure are collinear with the Ln^{3+}, being displaced from the Ln^{3+} by only half the length of the *c*-axis. Except for their distances from the $(Q_2)^{2-}$ layers, Ln^{3+} and A^+ have the same coordination environment. This gives the $ALnQ_4$ phases a similarity to the known $ALnQ_2$ compounds which possess the α-$NaFeO_2$ structure type. In these $ALnQ_2$ phases, A^+ and Ln^{3+} also share the same coordination environment (octahedral in this case) and, like $ALnQ_4$, are segmented such that every alternate cation layer is exclusively A^+ or Ln^{3+}.

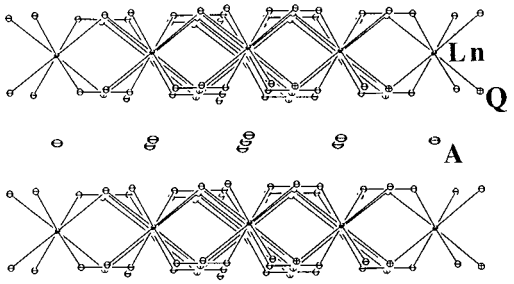

Figure 6. $ALnQ_4$ as seen parallel to the crystallographic [110] direction.

The change in structural dimensions when comparing the two $KLnSe_4$ analogues is consistent with the ionic radius of Tb^{3+} being smaller than that of Ce^{3+}. The cell volume of the Tb analogue is the smaller of the two (321.9(2) $Å^3$ vs 338.6(2) $Å^3$ for $KCeSe_4$), and the Ln−Se distances exhibit the expected changes as well (Tb−Se 2.980(1) Å; Ce−Se 3.075(1) Å). Both Ln−Se distances are consistent with the average values for the respective eight-coordinate Ln^{3+} which have been tabulated by Poix.[27] The changing bond lengths also make their presence felt on the respective Se−Se bonds. In $KTbSe_4$ the slightly stronger Tb−Se interaction results in a slightly longer Se−Se bond (2.393 Å). The bond angles respond somewhat to the change in Ln−Se distances as well; in general the Se−Ln−Se angles between Se atoms in the same plane are increased in the Tb analogue while the "trans-planar" angles are slightly smaller from those in $KCeSe_4$.

The repeating unit, shown in Figure 4, is the same unit which is found in two closely related three-dimensional structure types: $CuAl_2$ and $NbTe_4$. The former is seen in several compounds of the formula TX_2 (T = transition metal, X = Sb, Ge, Sn, or Pb)[28] and is simply the fusing of the anionic layers of $ALnQ_4$, through face-sharing at the square antiprisms, into a three-dimensional structure. Indeed, since A and Ln share coordination environments, $ALnQ_4$ can be considered as a derivative of the $CuAl_2$ structure type where the two cations alternate in the Cu positions along the *c*-axis. The $NbTe_4$ structure[29] is also closely related to that of $CuAl_2$; the Nb cations reside in half of the Cu positions and are ordered such that every other plane of metal positions is vacant, forming a porous structure. $NbTe_4$ has $(Te_2)^{2-}$ units, analogous to the $(Q_2)^{2-}$ units in $ALnQ_4$.

The known chemical similarities between all members of the lanthanide group would tend to indicate that other elements in this family could also be accommodated in the $ALnQ_4$ structure type. Such possibilities were, in fact, investigated. When Ln = La and Q = Se,

(27) Poix, P. *C. R. Acad. Sci. Paris Sec. C* **1970**, *270*, 1852−1853.
(28) Hulliger, F. *Struct. Bonding* **1968**, *4*, 83−229.
(29) Selte, K.; Kjekshus, A. *Acta Chem. Scand.* **1964**, *18*, 690−696.

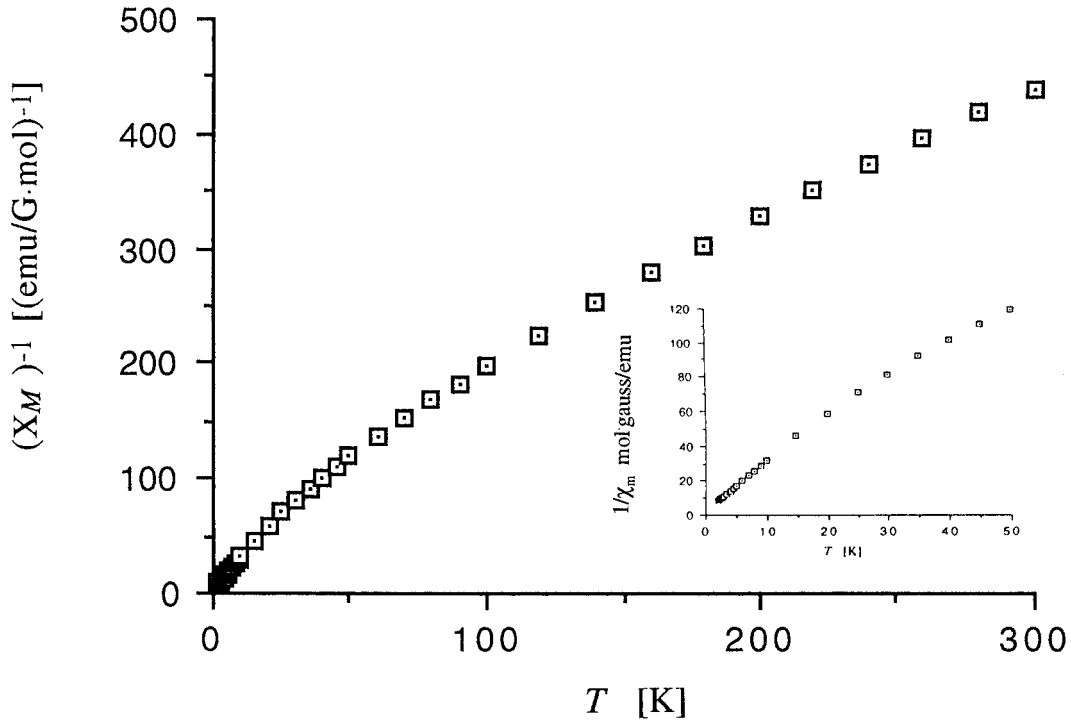

Figure 7. Inverse molar magnetic susceptibility ($1/\chi_M$) plotted against temperature (2−300 K) for $KCeSe_4$ (300 G). The inset graph shows an expanded view of the region 2−50 K.

reactions analogous to those described resulted only in $LaSe_2$. Phases with powder X-ray diffraction patterns similar to $ALnQ_4$ were isolated from reactions where A = K, Ln = Nd or Eu, and Q = Se, but these were consistently contaminated with large amounts of amorphous powder of a binary phase.

Magnetic Properties. The magnetic susceptibility of $KCeSe_4$ was measured from 2 to 300 K at 300 G, and a plot of $1/\chi_M$ vs T is shown in Figure 7. The material appears to be paramagnetic although several anomalies in the data are present. At temperatures below 100 K, the curve is seen to deviate negatively from a straight line extrapolated from the higher temperature data. Such deviation has been reported for several Ce^{3+} compounds and has been attributed to crystal field splitting of the cation's $^2F_{5/2}$ ground state.[30] At temperatures above 100 K, Curie−Weiss law is not strictly adhered to, and a slight curvature remains in the data. In this temperature range an average μ_{eff} of 2.3 ± 0.2 μ_B has been calculated. This value is in accordance with the usual range for Ce^{3+} compounds (2.3−2.5 μ_B) and is close to that of the free ion (2.54 μ_B). This magnitude of μ_{eff} is due to the shielding effect the outer electron cloud has on the embedded f-orbitals.[31] It was found that the measurements on $KCeSe_4$ must be done on freshly isolated sample, as a probable phase change in aged samples gives artificially high values for the μ_{eff}. This phase change probably occurs to a small extent on the sample surface because the bulk of the sample remains intact by X-ray powder diffraction.

The temperature-dependent magnetic susceptibility of $KTbSe_4$ proved to be of nearly ideal Curie−Weiss behavior with only a slight deviation from linearity beginning below 50 K (Figure 8). Above this temperature, a μ_{eff} of 9.25 ± 0.04 μ_B was estimated by applying a straight-line curve fit to the data from several trials.

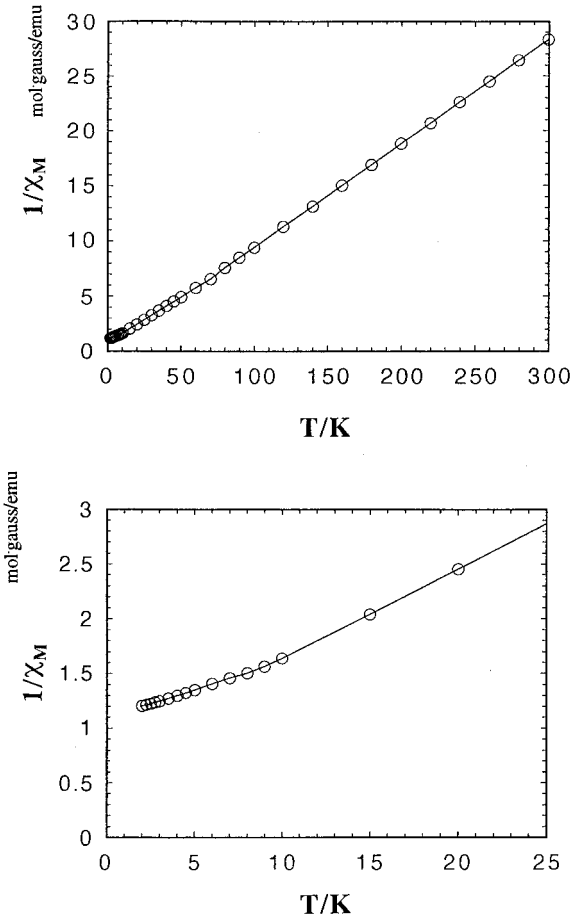

Figure 8. Top: Inverse molar magnetic susceptibility ($1/\chi_M$) plotted against temperature (2−300 K) for $KTbSe_4$ (5000 G). Bottom: expanded view of the region 2−25 K.

(30) (a) Lueken, H.; Bruggemann, W.; Bronger, W.; Fleischhauer, J. *J. Less Common Met.* **1979**, *65*, 79−88. (b) Duczmal, M.; Pawlak, L. *J. Magn. Magn. Mater.* **1988**, *76−77*, 195−196.

(31) Greenwood, N. N.; Earnshaw, A. *Chemistry of the Elements*; Pergamon Press: New York, 1984; p 1443.

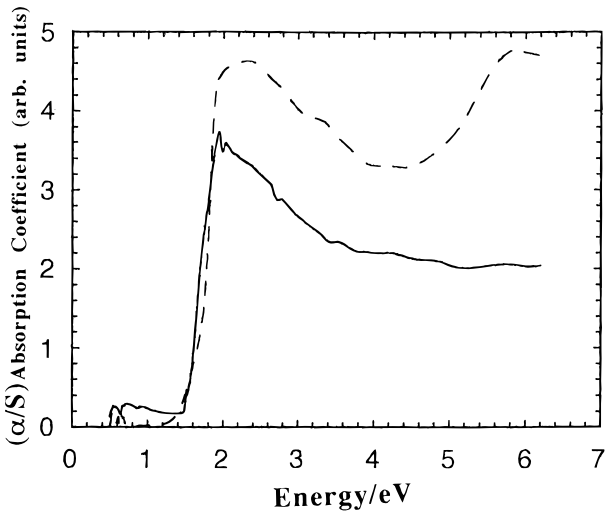

Figure 9. Solid-state diffuse reflectance spectra of $KCeSe_4$ (solid line) and $KTbSe_4$ (dashed line) plotted as absorption coefficient (a/S) vs energy (eV).

The calculated μ_{eff} of a Tb^{3+} cation (based on the $^7F_6$ ground state) is 9.72 μ_B with typically observed experimental values being 9.5−9.8 μ_B.[32] Also the small value of θ (ca. −6 K) indicates that the cation is much less prone to crystal field effects in this environment than is Ce^{3+}.[32]

Spectroscopy. A solid-state far-IR spectrum of $KCeSe_4$ shows no peaks, the only feature being a broad absorbance beginning at 250 cm^{-1}. The presence of this sort of feature is common in metallic materials, and so a four-probe conductivity measurement on a pressed pellet was performed at 300 K. A value of 5.1×10^{-6} S/cm was found, however, indicating a semiconducting material.

The solid-state far-IR spectrum of $KTbSe_4$ was somewhat more informative. A strong peak is clearly present at 151 cm^{-1}, which because of its low energy can be safely assigned as a Tb−Se vibration. Two broad peaks are evident at 370 and 515 cm^{-1} with a weak peak at 436 and a series of shoulders on the 370 peak at 325, 268, 227, and 201 cm^{-1}. Although tending to have a broad absorbance similar to that of $KCeSe_4$, the weak shoulders are all in a region where one would expect either Se−Se vibration energy (325 and 268 cm^{-1}) or slightly higher energy modes from the Tb−Se bonds (227 and 201 cm^{-1}).

The solid-state diffuse reflectance spectra of both compounds are shown in Figure 9. The sharp changes in α/S vs energy (eV) in the spectra of these materials correspond to estimates of the their bandgaps at 1.54 eV for $KCeSe_4$ and 1.65 eV for $KTbSe_4$. This helps to confirm that both are valence precise semiconductors. Simply on the basis of color one would expect the respective bandgaps as $KCeSe_4$ is a dark blue material while $KTbSe_4$ is dark purple. Although extrapolation of the absorption edges gives slightly different bandgaps for the two compounds, within experimental error, they are nearly identical.

$NaLnS_3$ (Ln = La, Ce). *Structure.* As in the structure of $KLnSe_4$, $NaLnS_3$ possesses anionic Ln/Q layers charge balanced with A^+ in the interlayer gallery.

(32) Casey, A. T.; Mitra, S. In *Theory and Applications of Molecular Paramagnetism*; Boudreaux, E. A., Mulay, L. M., Eds.; John Wiley and Sons: New York, 1976; p 306.

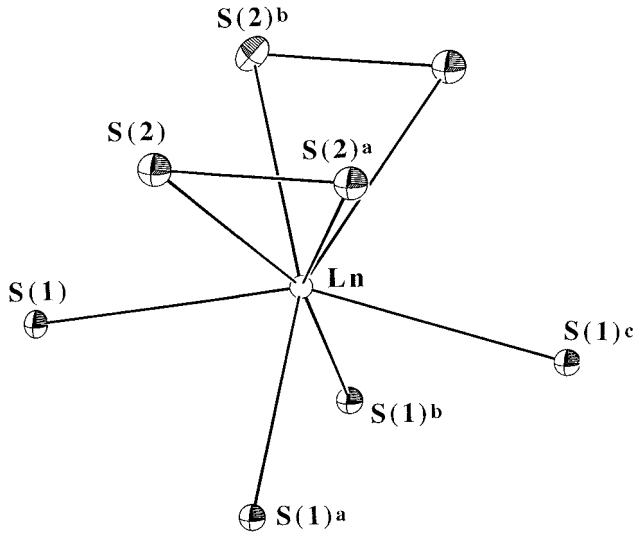

Figure 10. Immediate coordination environment of the Ln^{3+} cations in $NaLnS_3$ (Ln = La, Ce).

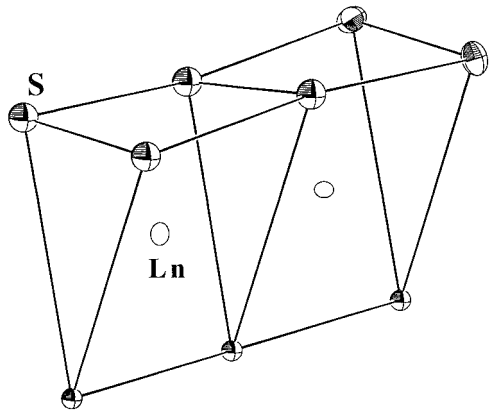

Figure 11. Face-sharing connection between two $[LnS_6]$ trigonal prisms featured in the structure of $NaLnS_3$.

The Ln^{3+} ions in $NaLnS_3$ are again 8-coordinate but now reside in bicapped trigonal prisms of S atoms made of two $(S_2)^{2-}$ units forming the short sides of the prism and four S^{2-} ions at the apex and capping positions (Figure 10). The coordination sphere about the Ln^{3+} is nearly identical for either La or Ce, except for the slightly larger bond distances in the La analogue due to the cation's slightly larger size.

The trigonal prisms of $NaLnS_3$ stack in one dimension by sharing triangular faces (Figure 11), forming chains parallel to the *c*-axis. Layers are formed when neighboring chains share monosulfides; this is done such that the monosulfides of the trigonal prisms in one chain are the capping monosulfides of the neighboring chains (Figure 12). This results in the $(LnS_3)_n^{n-}$ portion of the structure being analogous to the known phase, $ZrSe_3$; however, $ZrSe_3$ exhibits elongated Zr−Se bonds between the chains (Zr−Se = 2.72−2.74 Å within the chain, Zr−Se = 2.87 Å between the chains).[9] The larger coordination spheres of the Ln cations easily accommodate the eight sulfur atoms, and in fact, the capping bonds are no longer than any of the other Ln−S bonds present (see Tables 7 and 8).

The Ce−S distances for $NaCeS_3$ range from 2.838(1) to 3.010(1) Å and are comparable with those in previously reported compounds (2.878 Å in $KCeS_2$,[10g] 2.88−3.26 Å in CeS_2[33]). The disulfide bond of 2.105(3) Å is also reasonable. In $NaLaS_3$, the corresponding range

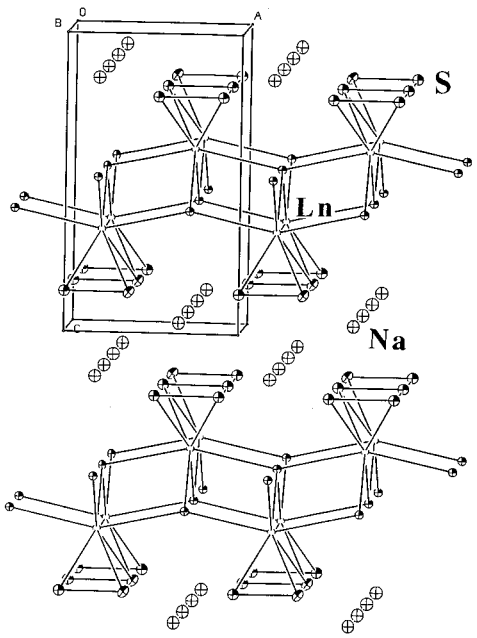

Figure 12. Extended structure of $NaLnS_3$ as seen parallel to the *b*-axis (circles with nonshaded octants: Na; open circles: Ln; circles with shaded octants: S).

Table 7. Selected Bond Distances (Å) and Angles (deg) for $NaLaS_3$ with Standard Deviations in Parentheses

La−S(1)	2.941(2)	S(2)−S(2)′	2.107(3)
La−S(1)′	2.869(1)	Na−S(2)	2.910(1)
La−S(2)	3.039(1)		
S(1)−La−S(1)[a]	81.99(2)	S(1)[a]−La−S(2)	83.55(3)
S(1)−La−S(1)[c]	155.86(7)	S(1)[a]−La−S(2)[b]	159.71(3)
S(1)[a]−La−S(1)[b]	96.47(6)	S(2)−La−S(2)[a]	40.57(5)
S(1)−La−S(2)	77.91(4)	S(2)−La−S(2)[b]	89.50(5)
S(1)−La−S(2)[a]	117.94(3)	S(2)[a]−La−S(2)[b]	103.40(5)

Table 8. Selected Bond Distances (Å) and Angles (deg) for $NaCeS_3$ with Standard Deviations in Parentheses

Ce−S(1)	2.9091(7)	S(2)−S(2)′	2.105(3)
Ce−S(1)′	2.838(1)	Na−S(2)	2.884(2)
Ce−S(2)	3.010(1)		
S(1)−Ce−S(1)[a]	81.80(2)	S(1)[a]−Ce−S(2)	83.44(4)
S(1)−Ce−S(1)[c]	155.25(7)	S(1)[a]−Ce−S(2)[b]	159.53(3)
S(1)[a]−Ce−S(1)[b]	96.58(6)	S(2)−Ce−S(2)[a]	40.93(5)
S(1)−Ce−S(2)	77.93(4)	S(2)−Ce−S(2)[b]	89.50(5)
S(1)−Ce−S(2)[a]	118.29(3)	S(2)[a]−Ce−S(2)[b]	103.64(5)

is from 2.869(1) to 3.039 Å, and the disulfide bond is nearly identical at 2.107(3) Å.

$NaLnS_3$ has some of the same structural motifs of the known Ln/Q_x binary systems which were discussed in the introduction as, for example, the structure of CeS_2[33] and that of $LnTe_3$. In that phase, the Ce^{3+} atoms are in an unusual nine-coordinate environment shown schematically in Figure 13. On one side of the lanthanide are the five monosulfides of the Ln^{3+}/Q^{2-} bilayer. On the opposite side of its coordination sphere, the Ce cation makes four bonds to three disulfides; two bonds are to both atoms of a disulfide while two more are to sulfur atoms from two separate disulfide units. The Ln^{3+}/Q^{2-} bilayer is sandwiched between layers of disulfide units in both cases, albeit with different coordination patterns to the lanthanides. While the binary compounds possess the alternating bilayer/disulfide motif, the new ternary materials have both an extra layer of disulfides (reminiscent of the pattern in the $LnTe_3$ phases) and an extra bilayer of Na cations (Figure 13). In the $LnTe_3$ phases there is a flat square net of tellurium atoms sandwiched between distorted rock-salt layers of $[LnTe]^{n+}$. In $NaLnS_3$ the corresponding square chalcogen net is strongly distorted into discrete S_2^{2-} units, and their bonding interaction with the distorted rock-salt layers of $[LnS]^{n+}$ is enhanced.

Recently, it has been reported that the Ln/Q framework of the $NaLnS_3$ structure type can also be stabilized by a mixture of K^+ and Cu^+ in the phase $KCuCe_2S_6$.[18] This quaternary phase features a monolayer of alkali cations between the anionic layers and Cu^+ ions residing in tetrahedral sites between the stacks of trigonal prisms. $KCuCe_2S_6$ has the further interesting feature that only one full Cu^+ atom is disordered over two separate crystallographic sites that alternate down the intralayer "groove". This disorder implied both Cu^+ mobility in the quaternary phase and that the related phases $KCeS_3$ and $CuCeS_3$ may be possible. The isolation of the $NaLnS_3$ phases lends credence to both these speculations by demonstrating the stability of the Ln/S framework. Further comparisons between the ternary and quaternary compounds will be made in a subsequent report detailing the synthesis and properties of three more members of this class of compounds: $KCuLa_2S_6$, $CsCuCe_2S_6$, and $KCuCe_2Se_6$.[18b]

Magnetic Susceptibility. The temperature-dependent magnetic susceptibility response of $NaCeS_3$ at 2000 G is shown in Figure 14. Despite the change in chalcogenide environment, the magnetic behavior of the Ce^{3+} remains similar to that seen in $KCeSe_4$: a Curie−Weiss paramagnet at high temperatures with deviations caused by crystal field splitting ensuing as the temperature drops. Above the onset of deviation, an μ_{eff} of 2.3 ± 0.2 μ_B and a Θ of -71 ± 1 K were estimated by fitting a straight line to the data. Again the μ_{eff} is close to that calculated for the free ion, consistent with the known insensitivity of f-orbitals to chemical environments. The magnetic response of $NaLaS_3$ was not investigated as La^{3+} is an f^0 cation and so is expected to be diamagnetic.

Spectroscopy. As would be expected from their isostructural nature, the solid-state far-IR spectra of $NaCeS_3$ and $NaLaS_3$ are very similar, with only the frequencies of the peaks shifting in response to the slight mass difference between the two lanthanides. Both materials show a strong peak in the region corresponding to S−S vibrations (493 cm^{-1} for $NaCeS_3$ and 490 cm^{-1} for $NaLaS_3$). A manifold of strong overlapping peaks is seen at lower energies which have been assigned as the Ln−S vibrations of their respective compounds. In $NaCeS_3$ these peaks are at 277, 243, 218, 193, and 177 cm^{-1} and a final, and much weaker peak exists at 137 cm^{-1}. The peaks of the corresponding manifold in $NaLaS_3$ are at 276, 241, 209, 188, 174, and 137 cm^{-1}.

The solid-state diffuse reflectance spectra of $NaCeS_3$ and $NaLaS_3$ are shown in Figure 15. The difference in color of the two phases is clearly evident in the change in bandgap between the two. The red $NaCeS_3$ exhibits a bandgap of 2.15 eV while the yellow La analogue one of 2.61 eV. $NaCeS_3$ has a considerable tailing below the initial absorption edge, which suggests either sample

(33) (a) Marsh, R. E.; Herbstein, F. H. *Acta Crystallogr.* **1983**, *39B*, 280−287. (b) Yanagisawa, Y.; Kanamaru, F.; Kume, S. *Acta Crystallogr.* **1979**, *35B*, 137−139.

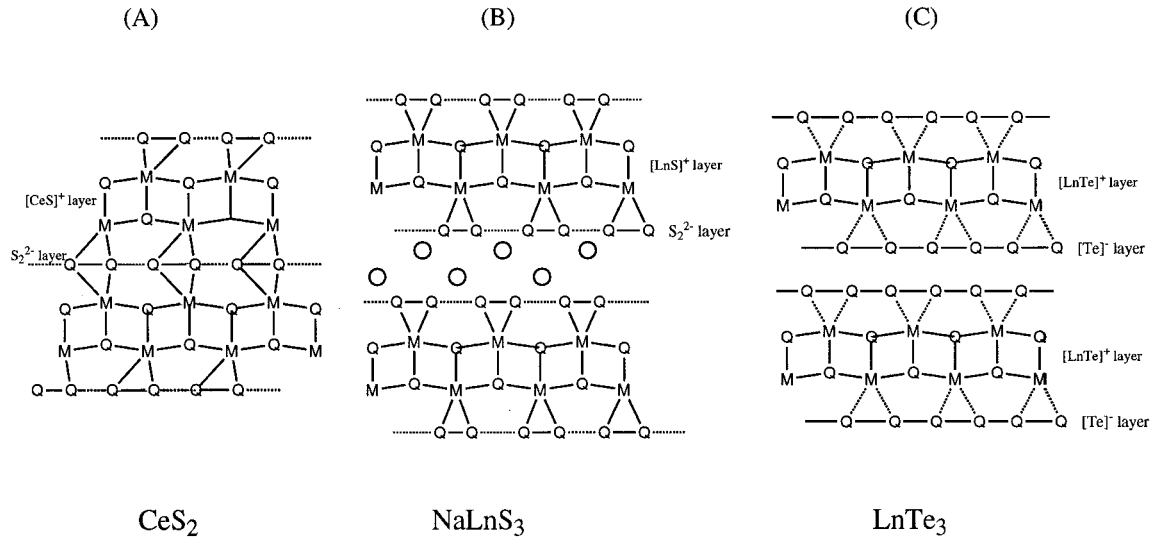

Figure 13. Schematic comparative drawings highlight the relationship between the (A) CeS_2, (B) $NaLnS_3$ and (C) $LnTe_3$, structures. The edge sharing rhombi represent distorted bilayers of the rock-salt $[LnQ]^{n+}$; the solid lines, sheets of $(Q_n)^{n-}$; and the open circles, Na^+ cations.

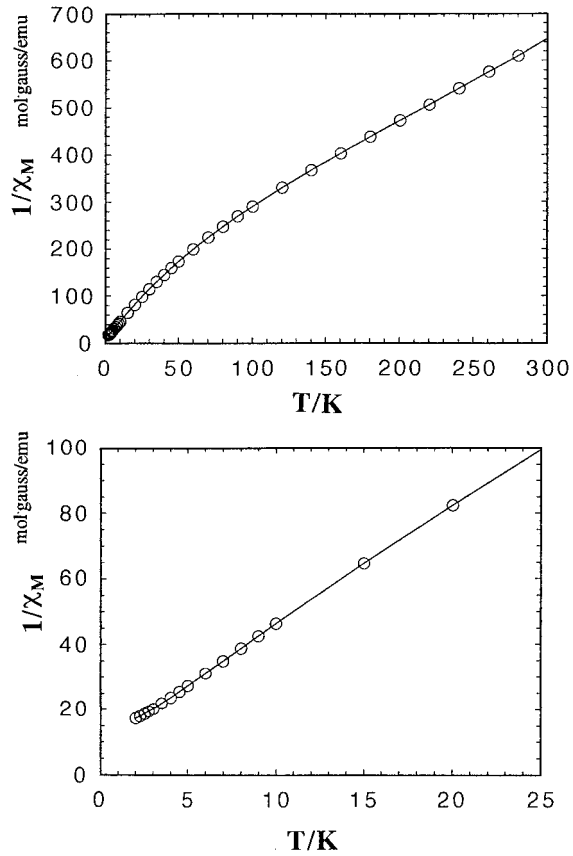

Figure 14. Inverse molar magnetic susceptibility ($1/\chi_M$) plotted against temperature (2−300 K) for $NaCeS_3$ (2000 G). (B) shows an expanded view of the region 2−25 K.

impurity or indirect character in the material's bandgap. The difference in bandgap between the two suggests that it may be possible to produce solid solutions of the formula $NaLa_{1-x}Ce_xS_3$ in which the bandgap of the material would be tunable based on the lanthanide ratio. Preliminary synthetic investigation of such phases were made by reacting various ratios of La/Ce in the previously described flux reaction for the ternary phase. Although evidence for solid solution behavior was observed, the final products were not of uniform homogeneity.

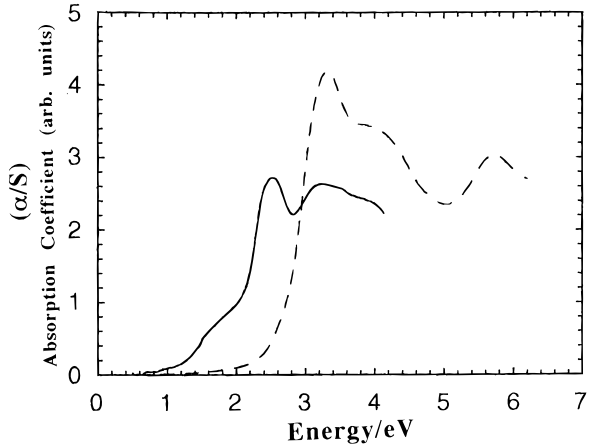

Figure 15. Solid-state diffuse reflectance spectra of $NaCeS_3$ (solid line) and $NaLaS_3$ (dashed line) plotted as absorption coefficient (α/S) vs energy (eV).

Conclusions

Although the conditions of the molten A_2Q_x flux have given rise to new phases in these systems, much of what has been described has some similarity to previously known f-block/chalcogenide chemistry. The most similarities were found in the $NaLnS_3$ structure type, which possesses several features closely related to those seen in the known polychalcogenide containing binaries. From a compositional standpoint, this is not too surprising because $NaLnS_3$ has only one equivalent of S more than LnQ_2, and it has exactly the same Ln/Q stoichiometry as the $LnTe_3$ phases. Because of the unique ability of Te to form infinite covalently bonded nets, the LnQ_3 phase had not been seen in either S or Se systems but distorted variants of it should be possible. The formation of a phase with increased amounts of S or Se becomes possible if some cationic species is available to balance the charge. With some help from Na, the Ln/S framework in $NaLnS_3$ merely expands along known structural themes.

The $ALnQ_4$ phases move slightly further from the known base of Ln/Q_x binaries while still retaining some similarities. There is no Ln/Q^{2-} bilayer here as there was in $NaLnS_3$; instead the Ln^{3+} cations are coordinated

directly and exclusively to $(Q_2)^{2-}$. Since both the $ALnQ_4$ and $NaLnS_3$ structure types have such strong relationships to the known binary compounds, it is likely that any further phases isolated from these systems will possess variations on the discussed structural themes.

The most chalcogenide-rich phase presented is, of course, K_4USe_8. Rather than forming an extended structure, the $[USe_8]^{4-}$ dodecahedron is stabilized. Actinides have a slightly greater covalent character to their bonding and higher charge than do the lanthanides. This may give an increased tendency to form discrete complexes, but it certainly does not preclude extended networks.

Acknowledgment. This research was made possible with funding from NSF Grant DMR-95-27347. M.G.K. is an A. P. Sloan Foundation Fellow and a Camille and Henry Dreyfus Teacher Scholar (1993−95). We thank Dr. J. H. Liao for help with the refinement of some of the structures. A.C.S. thanks the W. T. Pooh Foundation for support.

Supporting Information Available: Calculated and observed X-ray powder diffraction patterns, and anisotropic thermal parameters (13 pages); listings of calculated and observed structure factors for K_4USe_8, $KCeSe_4$, $KTbSe_4$, $RbCeTe_4$, $NaCeS_3$, and $NaLaS_3$ (10 pages). Ordering information is given on any current masthead page.

CM960448S